Stability of elastomeric isolation systems

I.G. Buckle & A. Itani

Department of Civil and Environmental Engineering, University of Nevada, Reno, United States of America

E. Monzon

California State University, Sacramento, United States of America

2017 NZSEE Conference

ABSTRACT: Elastomeric bearings with and without a lead core are commonly used as seismic isolators for protecting buildings, bridges and industrial plant from earthquakes However these devices have relatively low critical loads and those with slender geometry are believed to become unstable when subject to heavy axial load and simultaneously deformed to a high shear strain. But little experimental evidence exists to confirm the critical loads of these bearings and even less is known about the stability of a system of elastomeric bearings. In this paper an experimental investigation into the stability of a large-scale, curved, 3-span bridge model isolated by 12 lead-rubber bearings is described. The bridge was tested using the shake table array at the University of Nevada Reno. It was found that the horizontal curvature had little effect on the response of the isolators but it did cause asymmetry in the seismic response resulting in higher lateral displacements in the abutment isolators. Adequate vertical load capacity was maintained even at displacements exceeding the isolator diameter, when, by first-order theory, they should be unstable. Isolator instability at an abutment and a pier did occur at three times the design earthquake where the isolator shear strain was up to 400%. However, this instability did not cause the bridge superstructure to collapse because the isolators at other supports remained stable due to smaller imposed displacements. It has been shown that a system of isolators may remain stable even as individual isolators in that system become unstable.

1 INTRODUCTION

The classic solution for the critical load of a shear-flexible column such as an elastomeric bearing was developed by Haringx (1949). For bearings with high layer shape factors, Haringx gives the critical load for pinned-pinned end conditions (lateral displacement, Δ=0) as in Equation 1.

$$P_{cr,\Delta=0} = \pi\sqrt{K_r K_\theta} \tag{1}$$

where K_r is the shear stiffness of the bearing; and K_θ is the rotational stiffness. Various expressions have been suggested to obtain the critical load when the bearing is simultaneously deformed in shear ($\Delta\neq0$). The simplest, and that recommended in the AASHTO *Guide Specification for Isolation Design* (AASHTO, 2010), uses the overlap area method. In this case $P_{cr,\Delta}$ is given by:

$$P_{cr,\Delta} = P_{cr,D=0}\,\frac{A_r}{A_g} \tag{2}$$

where A_r is the area of the overlap between the upper and lower faces of the bearing; and A_g is the gross plan area of the bearing. This empirical equation has the advantage of simplicity but suggests the critical load of an elastomeric bearing is zero (i.e. unstable) when the shear displacement (Δ) is equal to the diameter of the bearing, i.e. when A_r = 0. This is assumed to be a conservative result but there is little experimental evidence to support this presumption.

In addition, there is no known experimental data on the stability of a system of elastomeric bearings that may be supporting a single structure such as a building or bridge. Instead it is often assumed that if one bearing is unstable, the entire system is unstable, despite the fact that axial loads and shear

displacements can vary widely throughout a system of isolators.

In this paper an experimental investigation into the stability of a 0.4-scale, curved, 3-span bridge model isolated by 12 lead-rubber bearings is described. The bridge was tested using the shake table array at the University of Nevada Reno

2 CURVED BRIDGE MODEL

2.1 Description

The prototype bridge is a three-span, composite steel I-girder bridge with a total subtended angle of 104° (1.8 radians). The components of this bridge were designed according to the AASHTO LRFD Bridge Design Specifications (AASHTO 2008). Seismic analysis was performed based on a spectrum defined by peak ground acceleration, *PGA*, of 0.47g, short-period spectral acceleration, S_s, of 1.14 g, and long-period spectral acceleration, S_1, of 0.41 g. The bridge was assumed to be located on a rock site (Site Class B) in Seismic Zone 3. A complete description of the design of the prototype bridge is given by Monzon et al. (2013).

The dimensions of the model were chosen to be the largest that could be accommodated within the physical limits of the Large-Scale Structures Laboratory, which measures 45.7 m by 15.2 m. Accordingly, a scale factor of 0.4 was chosen. The overall geometry of the prototype and the model is summarized in Table 1. Figure 1 shows the as-built bridge model in the laboratory.

Table 1. Major dimensions of prototype and model

	Prototype	**Model**
Total length (m)	110.5	44.2
Span lengths (m)	32.0, 46.5, 32.0	12.8, 18.6, 12.8
Centreline radius (m)	61.0	24.4
Total width (m)	9.15	3.66
Girder spacing (m)	3.4	1.37
Column height (m)	6.1	2.44
Column diameter (m)	1.52	0.62

The weight of the model superstructure was 1,215 kN, including the added mass needed for similitude. Each pier weighed 134 kN, and the total weight of the bridge model was therefore 1,483 kN.

2.2 Seismic isolators

Lead-rubber bearings (LRB) were used as the seismic isolators. These devices are relatively simple, have stable hysteretic properties, and have been implemented with success in many buildings and bridges. The characteristic strength, Q_d, and post-elastic stiffness, K_d, of the LRB isolators were determined such that the columns remained elastic during the design earthquake. The column moment at first yield (i.e. at the onset of yielding in any rebar) is equal to 383 kN-m, based on section analysis using the actual material properties. Assuming single curvature behaviour of the column, the shear force at first yield is 130 kN.

Analysis and design of the isolated bridge were performed following the procedure outlined in NCHRP Report 20-7 Task 262 (Buckle et al. 2011) and the provisions of the Guide Specifications for Seismic Isolation Design (AASHTO 2010). The isolator dimensions and properties are shown in Table 2. The pier isolators are larger than those at the abutments because of larger axial loads. The effective period of the bridge, calculated at the maximum isolator displacement during the design earthquake, was 1.16 s (the corresponding period of the prototype bridge was 1.85 s).

Figure 1. 0.4-scale curved bridge model; Left: View from above; Right: View from below

Table 2. Isolator dimensions and properties

	Abutment Isolators	**Pier Isolators**
Shear modulus, G (MPa)	0.41	0.41
Modulus of Elasticity, E (MPa)	1.24	1.24
Bonded diameter, B (mm)	191	229
Layer thickness, t_r (mm)	6.35	6.35
Number of layers, n	11	11
Total rubber thickness, T_r	70	70
Total height, H (mm)	178	178
Diameter lead core, d_L (mm)	32	38
Bonded area, A_b (mm^2)	27,711	39,903
Lateral stiffness, K_d (N/mm)	151	217
Characteristic strength, Q_d (kN)	6.27	9.03

3 EXPERIMENTAL SETUP

The two abutments and two piers were each supported on their own shake table. Earthquake ground motions were applied in the longitudinal (parallel to the chord) and transverse directions (x- and y-directions, respectively). The Sylmar (SYL) record from the 1994 Northridge Earthquake was used as the input motion. The major component (360 component), was applied in the longitudinal direction and the minor component, (090 component), in the transverse direction. In the experiment, the amplitude of the SYL record was scaled by 0.475 such that the S_1 of the 360 component was equal to that of the design spectrum. This scaled motion was considered to be the Design Earthquake (DE) for the purpose of the experiment. It was applied in increments of 10%, 20%, 50%, 75%, 100%, 150%, 200%, 250%, and 300%. The 150% DE was considered to be the Maximum Considered Earthquake (MCE). In the experiment, the time axis of the SYL motions was scaled by $\sqrt{S_L} = \sqrt{(1/0.4)} = 1.581$.

4 BRIDGE RESPONSE

4.1 Deck displacements

The maximum deck displacements at the middle of the bridge for each earthquake level are shown in Figure 2a. The displacements in the x-direction, u_x, and in the y-direction, u_y, increase nonlinearly with the earthquake level. The nonlinear increase of u_x is less apparent than that of u_y. This nonlinearity is expected because the effective stiffness of the isolation system is reduced as the displacement increases with increasing earthquake level. This reduction in stiffness results in period increase and an additional increase in displacement. The increase in period is apparent in Figure 2b where the u_x

displacement history from 100%, 150%, and 250% DE are shown in one plot. It can be observed that the period increases from 1.0 sec at 100% DE to 1.4 sec at 250% DE. The nonlinearity in u_y is more pronounced due to in-plane deck rotation, and is more apparent in the deck transverse displacements at abutments, as discussed below. The u_y displacement is smaller than u_x at all earthquake levels because the minor component of the ground motion was applied in the transverse direction.

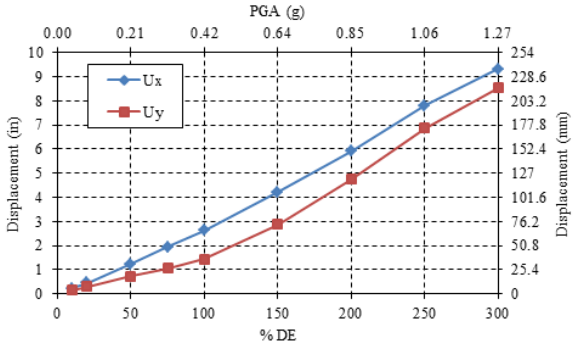

Figure 2a. Maximum deck displacements (u_x and u_y) at centre of bridge

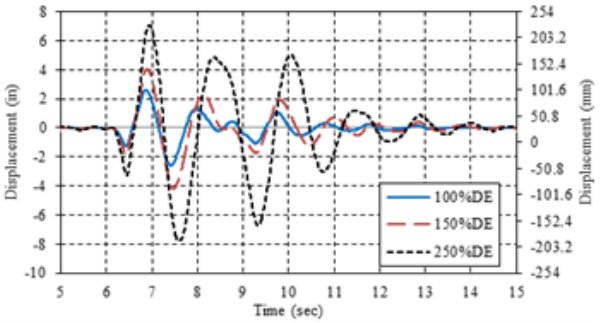

Figure 2b. U_x displacement history at centre of bridge

4.2 Deck rotations

Due to the eccentricity between the centre of mass and centre of stiffness of a curved bridge, lateral loading causes in-plane rotation of the deck, as illustrated in Figure 3. As a consequence, one end of the bridge experiences larger in-plane displacements than the other end. Assuming the superstructure behaves as a rigid diaphragm in its own plane, this rotation can be calculated as follows:

$$\theta_{deck} = sin^{-1}\left(\frac{\Delta_{y1} - \Delta_{y2}}{L_{chord}}\right) \quad (3)$$

where Δ_{y1} and Δ_{y2} are the transverse displacements of the two ends of the bridge (A1 and A4); and L_{chord} is the chord distance between these two points.

Longitudinal and transverse displacements at any point i on the deck due to θ_{deck} can be found from Equations 4 and 5:

$$u_{xi} = y_i \theta_{deck} \quad (4)$$

$$u_{yi} = x_i \theta_{deck} \quad (5)$$

where x_i and y_i are the longitudinal and transverse distances of point i from the centre of stiffness (C.K in Figure 3).

The effect of deck rotation on the longitudinal displacement (u_{xi}) is small because both θ_{deck} and y_i are small. However, the effect of deck rotation on the transverse displacement (u_{yi}) is large because despite θ_{deck} being small, x_i is large, and particularly so at the abutments.

4.3 Isolator displacements

Maximum resultant isolator displacements are shown in Figure 4. The trend of the isolator displacement is the same as the deck displacement. At the abutments, the isolator displacement is equal to the deck displacement because the support cross-frames are stiff and the forces were not high enough to cause girder rotations. However, at the piers, the deck displacement is equal to the sum of the isolator and column displacement due to column flexibility. The A1 isolators experienced the largest displacement, as shown in Figure 4 due to asymmetric response of the bridge. This implies that the abutment isolators in a curved bridge are the most susceptible to instability. Of the pier isolators, those located at P2 are the most susceptible for the same reason (larger displacements than at P3).

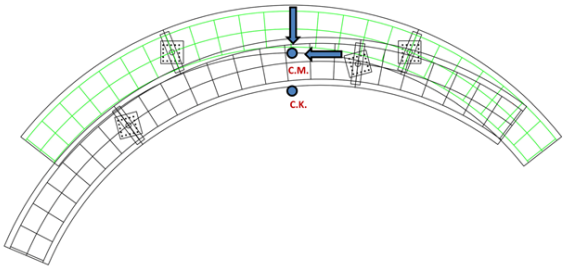

Figure 3. Displaced shape of curved bridge due to lateral loading at centre of mass (CM)

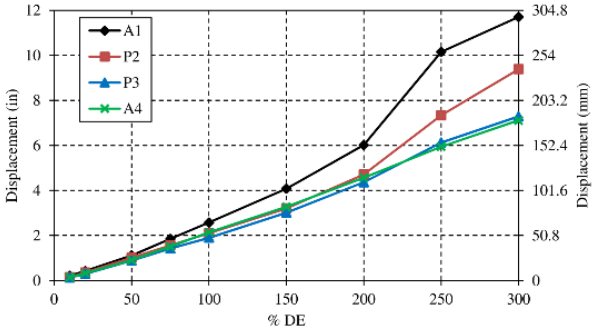

Figure 4. Resultant isolator displacements

4.4 **Vertical load instability**

The vertical load capacity of an elastomeric isolator such as an LRB decreases as the lateral displacement increases (Buckle et al. 2002; Kelly and Konstatinidis 2011; Sanchez et al. 2014). As noted in the introduction, this reduction in capacity is usually calculated by the overlap area (A_r) method, which implies that when the displacement is larger than the diameter and A_r is zero or negative, the isolator is unstable. See Equation 2.

As seen in Figure 4, at 250% DE, the displacement of the A1 isolators was about 250 mm. Although this is 33% larger than the isolator diameter, instability was not observed indicating that the isolators have much higher vertical load capacity than predicted by Equation 2.

Vertical load instability did however occur in the A1 isolators during the 300% DE run. In fact it occurred three times: at 7.735 s, 8.610 s, and 9.415 s (referred herein as B#1, B#2, and B#3, respectively). Screenshots from a video of the inside A1 isolator at the start, during instability, and at the end of the 300% DE SYL Run are shown in Figure 5.

The first peak with significant u_t displacement occurred at $t = 6.969$ *s*. The displacement was 512 mm, which is equivalent to shear strain of 318%. Even though this is larger than the isolator bonded diameter, instability did not occur as can be observed in Figure 5b.

The next peak displacement occurred at $t = 7.735$ *s* with u_t displacement of -267 mm, corresponding to shear strain of 382%. This is the first instance of instability in the A1 isolators, B#1, as shown in Figure 5c. It can be seen in this photo that the isolator 'sat down' on the bottom plate and, at the same time, the top plate was resting on the side of the isolator. Figure 5d shows a black mark on the top plate indicating it has been in contact with the side of the isolator. The instability was the result of excessive displacement combined with the vertical load acting on the isolators.

At the next cycle, the peak displacement occurred at $t = 8.601$ *s* with u_t displacement of 296 mm, equivalent to shear strain of 424%. Although Figure 5d shows that the inside isolator remains stable, the outside isolator did become unstable at this time, hence it is referred to as instability B#2. Examination of the isolators after the test again shows a black mark on the south side of the top plate (see Figure 5a for the north and south directions) similar to the marking shown in Figure 5d.

At the next cycle, the A1 isolators became unstable again at $t = 9.415$ *s* (B#3), as shown in Figure 5e. This was at the peak u_t displacement of -277 mm, which is about the same as the u_t displacement during instability B#1.

It is important to note that, even though the isolators were unstable on three occasions, the superstructure did not collapse, and no residual displacement was observed at the end of motion, as shown in Figure 5f. The reason for this behaviour is described in Section 4.5

It is noted that similar behaviour was observed in the Pier P2 isolators.

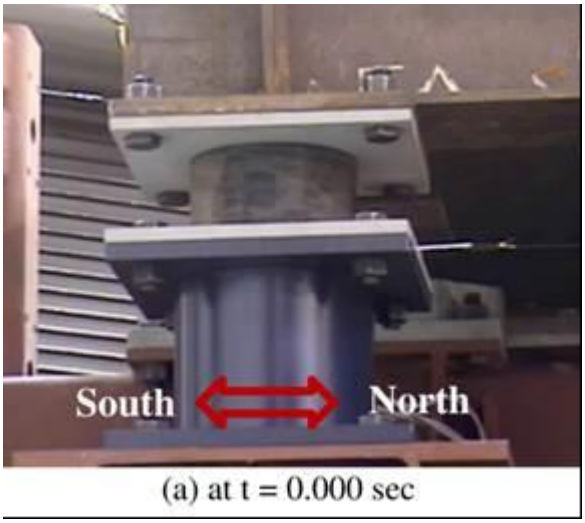

(a) at t = 0.000 sec

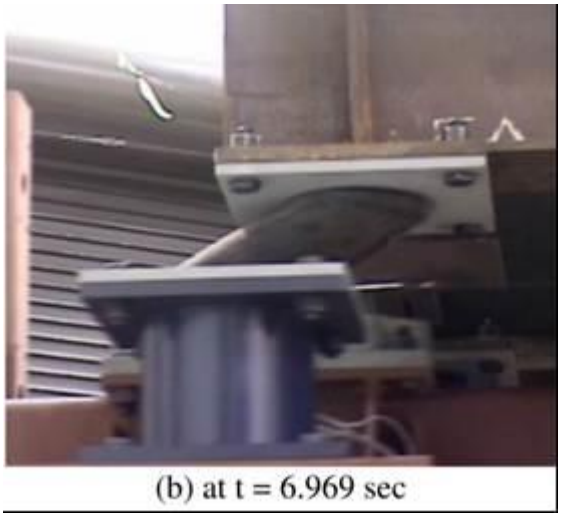

(b) at t = 6.969 sec

(c) at t = 7.735 sec – B#1

(d) at t = 8.601 sec – B#2

(e) at t = 9.415 sec – B#3

(f) at end of motion

Figure 5a-f. Screenshots from video of instability in abutment isolator A1 at t = 0 s, 6.969 s, 7.735 s, 8.601 s, 9.415 s and end

4.5 **Isolator hysteretic response**

Figure 6a shows the hysteresis loops for one of the isolators that became unstable at P2, for levels of excitation from 10% DE to 300% DE. Displacements up to 230 mm (9.0 in) are seen in the 300% DE Run. Clearly the isolator has become unstable during this Run as evidenced by segments of the loops with negative slopes and the overall reduction in the second slope (post-yield stiffness) to practically zero over almost the complete cycle of loading. This behaviour was typical of all six isolators on A1 and P2.

On the other hand Figure 6b shows the hysteresis loops for one of the isolators on P3 for the same levels of excitation. Here there is no evidence of instability, and this due to the fact that the maximum displacement in this isolator was only 140 mm (5.5 inches), which was significantly less than the isolator diameter. This behaviour was typical of all six isolators on P3 and A4.

It follows that of the 12 isolators supporting the superstructure, six became unstable during the 300%DE Run and six did not. Figure 6c shows the hysteresis loops for the entire bridge, i.e. it is the sum of all 12 isolator loops after transformation to a common coordinate system. No evidence of instability is seen in these loops and this is consistent with the observed behaviour that despite instability in some isolators, the bridge did not collapse but remained stable during the 300% DE Run.

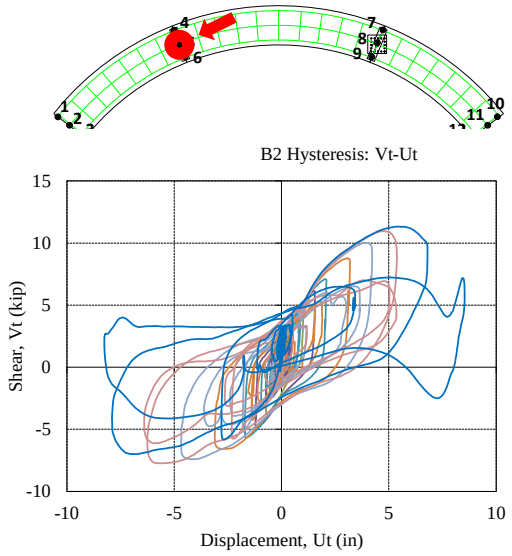

Figure 6a. Force displacement loop for isolator no. 5 at P2 for increasing levels of excitation showing unstable behaviour

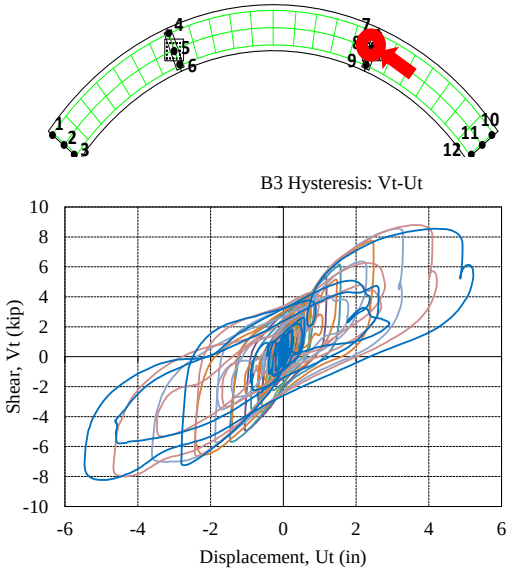

Figure 6b. Force displacement loop for isolator no. 8 at P3 for increasing levels of excitation showing stable behaviour

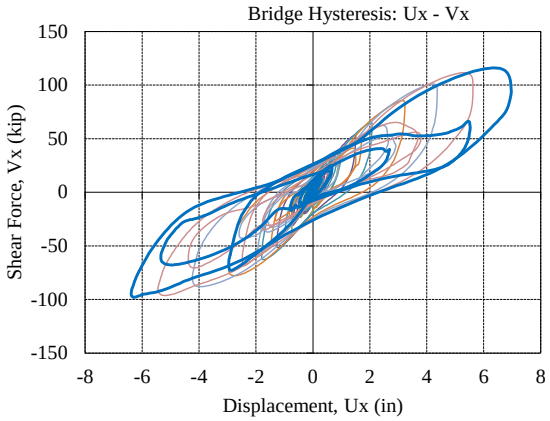

Figure 6c. Total force-displacement hysteresis loops summed over all 12 isolators for increasing levels of excitation showing stable behaviour of system

5 CONCLUSIONS

In this paper an experimental investigation into the stability of a large-scale, curved, 3-span bridge model isolated by 12 lead-rubber bearings has been described. The bridge was tested using the shake table array at the University of Nevada Reno. It was found that the horizontal curvature had little effect on the response of the isolators but it did cause asymmetry in the seismic response resulting in higher lateral displacements in the abutment isolators. Adequate vertical load capacity was maintained even at displacements exceeding the isolator diameter, when, by first-order theory, they should be unstable. Isolator instability at an abutment and a pier did occur at three times the design earthquake where the isolator shear strain was up to 400%. However, this instability did not cause the bridge to collapse because the isolators at other supports remained stable due to smaller imposed displacements. It has been shown that a system of isolators may remain stable even as individual isolators in that system become unstable.

Specifically, the following observations and conclusions are made:

- The seismic response of a symmetrical curved bridge is asymmetrical due to in-plane rotation of the superstructure. The deck in-plane rotation increases nonlinearly as the earthquake level increases due to bilinear properties of the isolators and non-uniform distribution of isolator and column displacements.
- The asymmetrical response caused by horizontal curvature subjected the isolators at one abutment to higher displacements than those over the piers or at the other abutment.
- The isolators have adequate vertical load capacity even at displacements larger than their diameter, when they should be unstable by first order methods of analysis.
- Instability of isolators at one abutment and an adjacent pier did not lead to bridge collapse.
- Repeated instability of isolators did not cause permanent deformation in the isolator or in the entire bridge
- Most likely explanation is that of the 12 isolators supporting this bridge only six became unstable due to excessive displacement and the remaining six were sufficiently stable that the overall system of 12 isolators was stable.

6 ACKNOWLEDGMENTS

This project was funded by the Federal Highway Administration under Contract DTFH61-07-C-00031. The technical oversight provided by the Contract Officer's Representatives (Dr Wen-huei (Phillip) Yen, Mr Fred Faridazar and Ms Shelia Duwadi) is gratefully acknowledged.

7 REFERENCES

AASHTO. (2008). *AASHTO LRFD Bridge Design Specifications*, AASHTO, Washington, DC.

AASHTO. (2010). *Guide Specifications for Seismic Isolation Design*, AASHTO, Washington, DC.

Buckle, I.G., Moustafa, A-A. & Monzon, E.V. (2011). *Seismic Isolation Design Examples of Highway Bridges*, Final Report, NCHRP 20-7/Task 262 (M2), Transportation Research Board, Washington, DC.

Buckle, I.G., Nagarajaiah, S. & Ferrell, K. (2002). Stability of Elastomeric Bearings: Experimental Study, *J. of Structural Engineering*, 128(1), 3-11.

Haringx, J.A. (1949). Phillips Research Report, 3, Phillips Research Laboratories, Eindhoven.

Kelly, J.M. & Konstantinidis, D. (2011). *Mechanics of Rubber Bearings for Seismic and Vibration Isolation*, John Wiley & Sons, UK.

Monzon, E.V., Buckle, I.G. & Itani, A.M. (2013). *Seismic Performance of Curved Steel Plate Girder Bridges with Seismic Isolation*, CCEER Report No. 13-06, Department of Civil and Environmental Engineering, University of Nevada, NV.

Sanchez, J., Masroor, A., Mosqueda, G. & Ryan, K. (2013). Static and Dynamic Stability of Elastomeric Bearings for the Seismic Protection of Structures, *J. of Structural Engineering*, 139(7) 1149-1159.